Tetrahedron 70 (2014) 2992–2998

Contents lists available at ScienceDirect

Tetrahedron

journal homepage: www.elsevier.com/locate/tet

Binaphthalene bridged bipolar transporting materials for blue electroluminescence: toward high EL efficiency via molecular tuning

Rossatorn Muangpaisal [a,b,c], Wei-I. Hung [b], Jiann T. Lin [b,*], San-Yu Ting [d], Li-Yin Chen [d,*]

[a] Taiwan International Graduate Program, Taiwan, ROC
[b] Institute of Chemistry, Academia Sinica, 128 Section 2 Academia Road, Nankang, Taipei 11529, Taiwan, ROC
[c] Department of Chemistry, National Tsing Hua University, 101 Section 2 Kuang-Fu Road, Hsinchu 30031, Taiwan, ROC
[d] Department of Photonics, National Sun Yat-Sen University, Kaohsiung 804, Taiwan, ROC

ARTICLE INFO

Article history:
Received 20 December 2013
Received in revised form 26 February 2014
Accepted 6 March 2014
Available online 16 March 2014

Keywords:
Amorphous materials
Blue light-emitting
Bipolar transport
Structure–properties correlations
Organic light emitting diode

ABSTRACT

Two isomeric bipolar transporting molecules containing arylamine and benzimidazole moieties linked by 1,1′-binaphthalene bridge have been synthesized and used for blue light-emitting diodes. The highly twisted binaphthalene bridge is beneficial for amorphous morphology, good solubility, high thermal stability and high photoluminescence quantum efficiency (Φ_{PL}). The charge transfer bands of these compounds exhibit interesting solvent-polarity dependent fluorescence properties. The physical properties of the compounds were tunable upon binding of the benzimidazole with binaphthalene group via *C*- (**BINAPC**) or *N*- (**BINAPN**) linkage. Three-layered blue-emitting OLEDs using **BINAPC** or **BINAPN** as the emitting layer, NPB as the hole transporting layer, and TPBI as the electron transporting layer as well as hole-blocking layer exhibit good performance. External quantum efficiencies of 2.49% with color coordinates of (0.15, 0.11) and 2.67% with color coordinates of (0.16, 0.16) were achieved for **BINAPC** and **BINAPN**, respectively.

1. Introduction

Organic light-emitting diodes (OLEDs) have potential applications in display and solid-state lighting.[1] In recent years, significant progress has been made on light-emitting materials for full color display and light source, including luminous efficiency, color purity, and lifetime.[2] Blue-, green-, and red-emitting materials provide three prime colors needed for OLEDs application. Though the development of red- and green-emitters for organic light emitting diodes (OLEDs) has been very satisfactory so far, progress on blue emitters with good stability and high efficiency still lag behind and there is much room for improvement in order to speed up light-emitting device technology.[3] Critical requirements for emissive materials in OLEDs include high luminescence quantum yield and color purity in the solid state, bipolar transport, good film morphology, and good thermal and redox stability.[2]

Both small molecules and polymers are commonly used as emitters of OLEDs. Compared to polymers, small molecules are easier to purify and have well-defined molecular weight. In contrast, small molecules have higher tendency to form crystals,[4] which frequently result in device failure. Therefore, proper design of small molecules for forming amorphous morphology is desired for OLEDs application. Moreover, amorphous materials with a high glass transition temperature have advantages over crystalline materials due to their good solubility and easy processability.[5] The binaphthalene entity is widely incorporated in molecules for sensor,[6] asymmetric catalysis,[7] non-linear optics,[8] and light-emitting diodes.[9] It was demonstrated that the binaphthalene moiety in a molecule could resist molecular crystallization and facilitate formation of glassy morphology.[10]

Our group has been interested in bipolar transporting materials because these molecules can more effectively confine excitons and improve the device performance and stability.[11] A straightforward design strategy for bipolar transporting molecules is to incorporate the hole- and electron-transporting moieties into a single molecule, i.e., the donor-acceptor type approach.[12] For blue emitters, the choice of suitable interconnection between the hole-transporting, electron-transporting, and π-conjugated spacer is crucial to avoid prominent bathochromic shift due to extended π-conjugation.[13] In 2011, Huang and co-workers reported bipolar blue-light emitting materials containing a hole-transporting triphenylamine moiety and an electron-transporting benzimidazole moiety at the C-9 and C-10 position of the anthracene.[14] By modified the number and position of phenyl bridge between functionalized moieties and anthracene core, the color and the energy levels of these materials were adjustable.

* Corresponding authors. Tel.: +886 2 27898522; fax: +886 2 27831237; e-mail addresses: jtlin@gate.sinica.edu.tw, jtlin@chem.sinica.edu.tw (J.T. Lin).

0040-4020/$ – see front matter © 2014 Elsevier Ltd. All rights reserved.
http://dx.doi.org/10.1016/j.tet.2014.03.017

In this work, we report the synthesis and investigation of two isomeric bipolar blue light-emitting molecules consisting of an electron-donating arylamine, an electron-accepting *N*-phenylbenzimidazole, and an in-between binaphthalene bridge. Zhao and co-workers reported that compounds with different π-conjugated isomeric structures exhibited different carrier transport behaviors in OTFTs.[15] The two isomers in this study differ in the interconnection mode of the electron-accepting *N*-phenylbenzimidazole entity to the binaphthalene bridge, i.e., via *C*- or *N*-linkage, are therefore expected to have different carrier transport properties. Blue OLEDs based on these materials will be also discussed. Some carbazole/benzimidazole hybrid molecules were studied recently by both experimental and computational approaches, and they appeared promising as the host materials for phosphorescent emitters.[11b,16]

2. Results and discussion

2.1. Synthesis

The synthesis of the target molecules is outlined in Scheme 1. Compounds **1a** and **1b** underwent Miyaura borylation reaction to afford **2a** and **2b**, respectively. Subsequent palladium-catalyzed Suzuki cross coupling reaction of **2a** and **2b** with 4′-bromo-*N*,*N*-diphenyl-[1,1′-binaphthalen]-4-amine provided the desired products. The isolated yields are 68% and 43% for **BINAPC** and **BINAPN**, respectively. The new compounds were fully characterized by ^{1}H and ^{13}C NMR spectra, mass spectra, and elemental analysis.

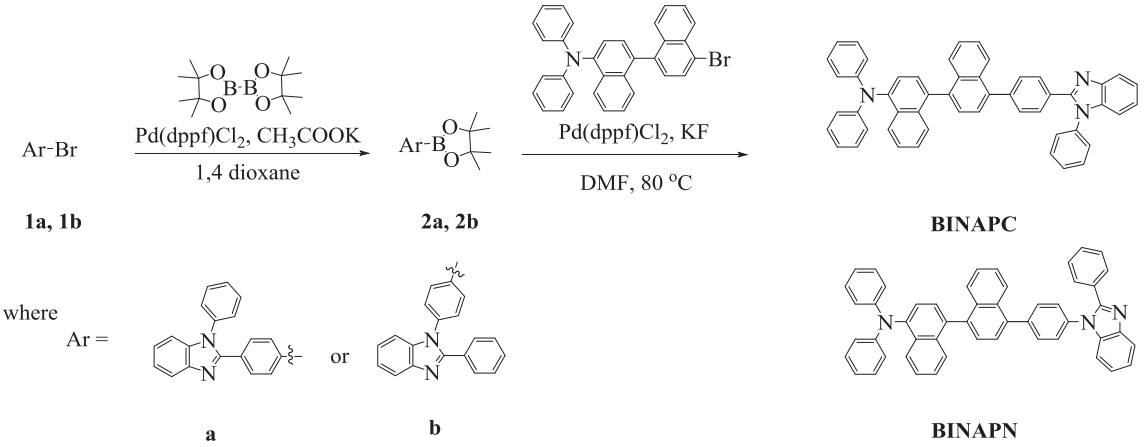

Scheme 1. Synthetic pathways of **BINAPC** and **BINAPN**.

hole- and electron-transport units, respectively. Extended conjugation of the arylamine entity may decrease its color purity.[17] Therefore, a bulky binaphthalene bridge was used to avoid strong charge transfer between the arylamine and the *N*-phenylbenzimidazole. The representative absorption and emission spectra of the compounds in dichloromethane and in the film cast on a glass substrate are shown in Fig. 1, and the photophysical data are summarized in Table 1.

Similar to the previously reported π-conjugated arylamine/benzimidazole compounds, the absorption peak around 300 nm can be attributed to amine-centered π–π* transition.[18] The band of longer wavelength is due to the charge transfer absorption from the diphenylamine to the benzimidazole group, which is in agreement with the theoretical computation (vide infra). The absorption intensity of the charge transfer band (~350–450 nm) is much lower than those of the congeners with different π-conjugated spacers.[11a] This outcome can be rationalized by the partial disruption of the π-conjugation caused by the binaphthalene group. In contrast, a saturated spacer can more effectively decouple the interaction of donor and acceptor and suppress the intramolecular charge transfer (ICT).[19]

Both compounds emit in the blue region upon excitation at 290 nm. The emission intensity of both compounds are linearly proportional to concentration in the range of 10^{-5} to 10^{-4} mol dm^{-3}, suggesting negligible aggregation of the dye molecules.[20] There is red shift of the fluorescence spectra upon increasing the solvent polarity (Fig. 2). The spectral shift can be correlated with the solvent

2.2. Thermal properties

The thermal properties of the new materials were investigated by TGA and DSC analyses in a nitrogen atmosphere. **BINAPC** and **BINAPN** possess very high thermal decomposition temperatures (5% weight loss) at 440 and 404 °C, respectively (Fig. S1; Supplementary data). No apparent exothermic crystallization and endothermic melting peaks were observed for both **BINAPC** and **BINAPN** from the DSC thermograms during heating and cooling cycles, indicating the amorphous nature of these binaphthalene bridge molecular solid.[9a] High thermal stability and amorphous characteristics of the compounds should be beneficial to their application in OLEDs.

2.3. Photophysical properties

The main purpose of this study is to construct molecules possessing bipolar carrier-transport properties and emitting in the blue region or at even shorter wavelengths. As aforementioned, the arylamine and *N*-phenylbenzimidazole entities were chosen for

polarity (Δf) and the difference of dipole moment between the ground and excited states according to the Lippert–Mataga equation (Eq. S1; Supplementary data).[21] The spectral shift is proportional to the solvent polarity, indicating the bipolar nature of the transition.[16a] The triplet energies (E_T) of both compounds, estimated from the highest energy peak of the phosphorescence taken in toluene at 77 K, were found to be ~2.2 eV. This value is high enough for the compounds to be used as the host for red phosphors in future studies.

2.4. Electrochemical properties

The electrochemical properties of **BINAPC** and **BINAPN** were investigated by cyclic voltammetry (CV). Both compounds exhibited a quasi-reversible wave due to the oxidation of the arylamine unit.[22] No reduction wave was detected. Representative cyclic voltammograms are shown in Fig. S3 (Supplementary data). The two compounds exhibited nearly identical oxidation potentials. The HOMO energy levels of the compounds were calculated to be −5.49 eV from cyclic voltammetry and by comparison with ferrocene (−4.8 eV,

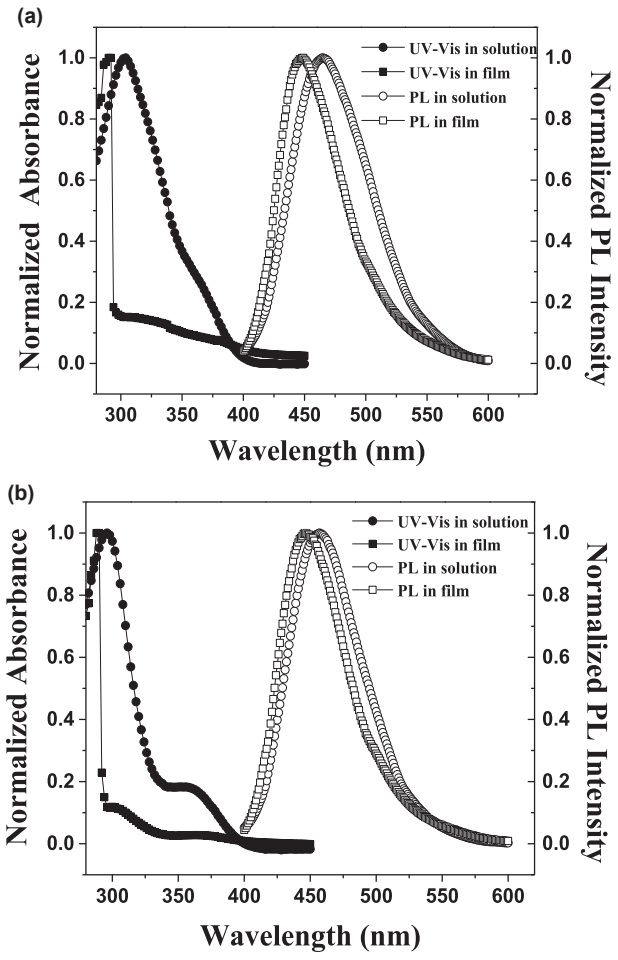

Fig. 1. Normalized UV–visible absorption and PL spectra of (a) **BINAPC** and (b) **BINAPN** in dichloromethane and in the film cast on the glass substrate.

Table 1
Physical data of **BINAPC** and **BINAPN**

Compound	T_g/T_d (°C)[a]	λ_{abs} (nm) [sol[b]/film]	λ_{em} (nm) [sol[b]/film]	Φ_{PL}[c]	HOMO/LUMO (eV)[d]	E_g[e]
BINAPC	–/440	304, 364/290	465/449	0.33	−5.84/−2.83	3.01
BINAPN	–/404	296, 352/290	457/446	0.45	−5.86/−2.80	3.06

[a] T_g: glass-transition temperature. T_d: thermal decomposition temperature. The heating and cooling rates were 10 and 30 °C min^{-1}, respectively.
[b] Absorption maximum and emission maximum measured in CH_2Cl_2.
[c] The PL quantum efficiency (Φ_{PL}) was measured in toluene solution using anthracene (Φ_{PL}=0.28 in ethanol) as the standard.[27]
[d] The HOMO energies were determined through AC II measurements; LUMO=HOMO+E_g.
[e] The value of E_g was calculated based on the absorption onset of the solid film.

below the vacuum level). As the HOMO energy calculated by CV method normally depends on the solvent used for the measurement, the atmospheric photoelectron spectroscopy was also used to estimate the HOMO energy of **BINAPC** and **BINAPN**. The HOMO energy of **BINAPC** estimated from the AC II measurements is slightly lower than that of **BINAPN** by ~0.02 eV.

2.5. Charge-transport properties

The carrier-transport properties of **BINAPC** and **BINAPN** were investigated by the time-of-flight (TOF) transient-photocurrent technique at room temperature. The TOF transient for electrons and holes of the compounds are shown in Fig. S4 (Supplementary data). From the intersection point of two asymptotes in the

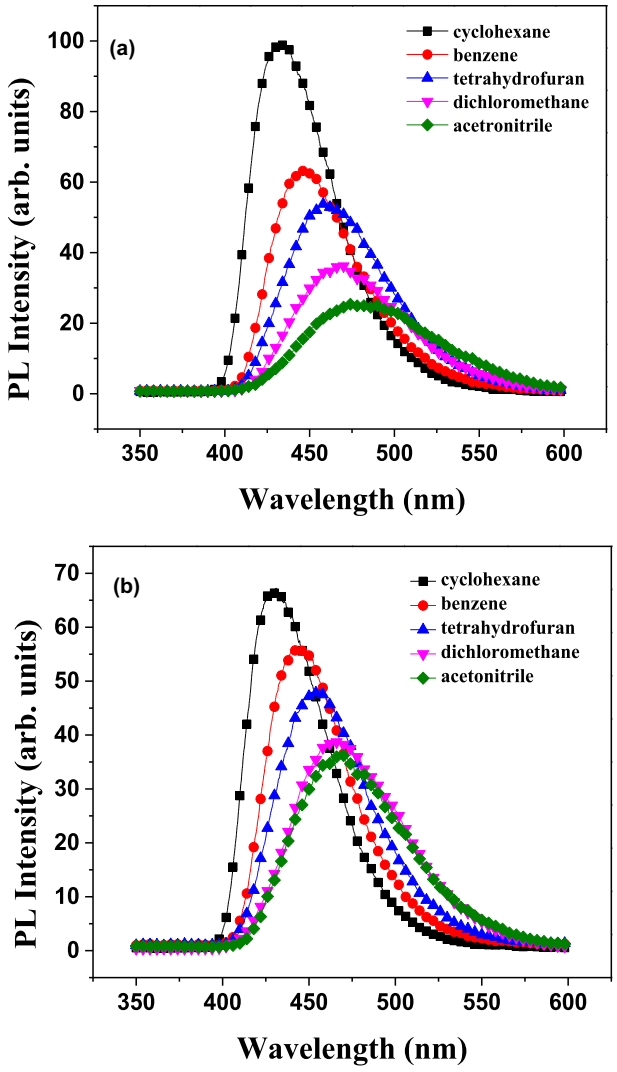

Fig. 2. PL spectra of (a) **BINAPC** and (b) **BINAPN** in various solvents.

double-logarithmic representation of the TOF transient, the carrier-transit time (t_T) needed to determine the carrier mobilities can be evaluated. The two compounds exhibit both electron- and hole-transport behavior, with dispersive transport characteristics. The field dependence of the carrier mobilities follows the nearly universal Poole–Frenkel relationship (Fig. S5, Supplementary data).[23] Relevant data for the electron and hole mobilities are shown in Table 2. In comparison, the hole mobilities of **BINAPC** and **BINAPN** are nearly three orders lower than that ($\sim 10^{-3}$ cm^2 V^{-1} s^{-1}) of commonly used diphenylamino-based hole-transport materials, 1,4-bis(1-naphthylphenylamino)-biphenyl (NPB).[24] In comparison, the electron mobilities of the two compounds are comparable to those of the typical electron-transport material, 1,3,5-tris(*N*-phenylbenzimidazol-2-yl)-benzene) (TPBI) ($\sim 10^{-5}$ cm^2 V^{-1} s^{-1}) and *N*-arylbenzimidazole-containing analogues ($\sim 10^{-5}$–10^{-6} cm^2 V^{-1} s^{-1}).[25] The hole mobility of **BINAPN** is about twice of that of **BINAPC**, while the electron mobility of **BINAPC** is more than four times higher than that of **BINAPN**. The two isomers in this study have the same trend in carrier mobility: they all have higher electron mobility than hole mobility. In **BINAPC**, the electron mobility is higher than hole mobility by ~2 order. The electron mobility and hole mobility of **BINAPN** are more balanced compared to those of **BINAPC**. The different behaviors for the two isomers are not unexpected, as the carrier mobilities of glassy materials are affected by both carrier-transport units and molecular geometries.[26]

Table 2
Electron and hole mobilities of compounds measured from the TOF method

	μ_e[a] ($cm^2\ V^{-1}\ s^{-1}$)	β[b] $(cm\ V^{-1})^{1/2}$	μ_h[a] ($cm^2\ V^{-1}\ s^{-1}$)	β[c] $(cm\ V^{-1})^{1/2}$	Electric field ($V\ cm^{-1}$)
BINAPC	5.4×10^{-6} (d)	7.85×10^{-3}	2.3×10^{-4} (d)	2.09×10^{-3}	6×10^{5}
BINAPN	1.2×10^{-5} (d)	1.54×10^{-3}	5.4×10^{-5} (d)	3.33×10^{-3}	5×10^{5}

[a] μ_e: electron mobility, μ_h: hole mobility; d: dispersive.
[b] Poole–Frenkel factor for the electron transport.
[c] Poole–Frenkel factor for the hole transport.

2.6. Theoretical calculation

Calculated density surfaces of the highest occupied molecular orbital (HOMO) and the lowest unoccupied molecular orbital (LUMO) are shown in Fig. 3. The HOMOs of both compounds are mainly located on the donor. Conversely, the structure factor accounts for the LUMOs located in different regions for the two compounds. The LUMO of **BINAPC** is distributed across the bridge and acceptor, whereas the LUMO of **BINAPN** is mainly distributed on the bridge. This is probably due to the difference in the dihedral angle between the phenyl and benzimidazole (ca. 30° for **BINAPC**; ca. 55° for **BINAPN**). Similar observation was reported on the carbazole/phenylbenzimidazole derivatives developed by Wong and co-workers.[16b]

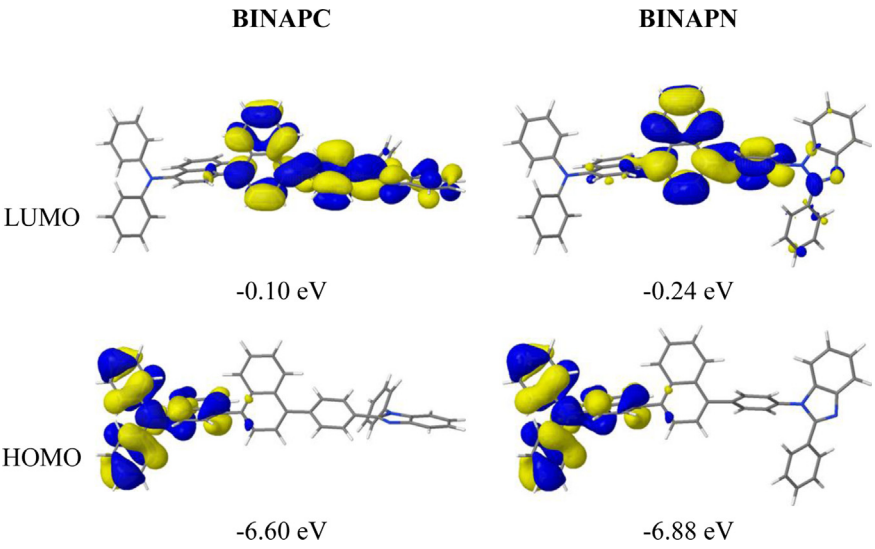

Fig. 3. Calculated density surfaces of the molecular orbitals of **BINAPC** (left) and **BINAPN** (right) at ωPBE/6-31G* level.

The simulated absorption spectra based on time-dependent calculations for **BINAPC** and **BINAPN** follow the same trend as that in experimental observation: **BINAPC** has more bathochromic charge transfer excitation (longer wavelength bands) and more hypsochromic localized excitation (shorter wavelength bands). The simulated absorption bands are shown in Fig. S7 (Supplementary data). The excitation energies of the $S_0 \rightarrow S_1$ transition after optimization of the excited state structure are similar for **BINAPC** and **BINAPN**, which is consistent with the similar emission wavelengths of the two isomers.

2.7. Electroluminescent properties and OLED characteristic

Based on the thermal, photophysical and carrier mobility properties, the new compounds appeared to be promising as non-doped blue-emitting materials for OLED application. Non-doped single-layer EL device I with structure of ITO/**BINAPC** or **BINAPN** (80 nm)/LiF (1 nm)/Al (100 nm) was first fabricated. However, the performance of the device I was far from satisfactory, despite of the bipolar transport behavior of the two compounds. Possibly dispersive transport characteristics of the compounds shorten the carrier lifetime in thicker films. Consequently, three-layer device II with a structure of ITO/NPB (30 nm)/**BINAPC** or **BINAPN** (20 nm)/TPBI (30 nm)/LiF (1 nm)/Al (100 nm) was fabricated. NPB and TPBI were used as the hole- and electron-transporting materials, respectively, while LiF and Al were used as the buffer layer and the cathode, respectively. NPB and TPBI were chosen for our purpose as the HOMO and LUMO energy levels of the compounds matched reasonably well with the HOMO and LUMO levels of **BINAPC** and **BINAPN**, respectively (Fig. 4). The performance parameters of these devices are collected in Table 3. Representative EL spectra, current–voltage–luminance (I–V–L) characteristics, and current–efficiency–voltage plots of these devices are shown in Fig. 5. When the thinner film of **BINAPC** or **BINAPN** used as the emitting layer, electrons, and holes are effectively confined in the emitting layers to form excitons. This is also supported by the nearly superimposable EL and PL spectra. The slightly better device performance of **BINAPN** than **BINAPC** may be due to the higher quantum yield and better balanced carrier mobility

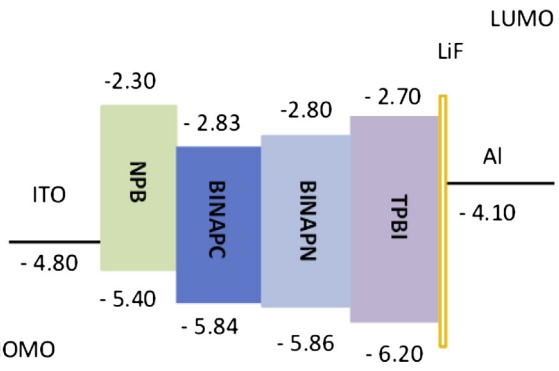

Fig. 4. Energy levels diagram of relevant materials used for device fabrication.

Table 3
Electroluminescent data of devices I and II

	BINAPC	BINAPN
V_{on} (V)[a]	9.5; 3.5	8.5; 4.0
L_{max} (cd m^{-2}) (V at L_{max}, V)[b]	57 (14.0); 12,448 (14.0)	32 (14.0); 15,250 (14.0)
λ_{em} (nm)[c]	464; 450	458; 458
CIE (x, y)[d]	0.16, 0.21; 0.15, 0.11	0.16, 0.17; 0.16, 0.16
FWHM (nm)[e]	88; 70	74; 72
$\eta_{ext,max}$ (%)[f]	0.08; 2.49	0.13; 2.67
$\eta_{p,max}$ (lm W^{-1})[g]	0.03; 1.98	0.04; 1.77
$\eta_{c,max}$ (cd A^{-1})[h]	0.13; 2.43	0.17; 3.32

[a] V_{on} (turn-on voltage) was obtained from the-intercept of the plot of log (luminance) against applied voltage.
[b] L: luminance; max: maximum.
[c] λ_{em}, λ maximum at emission wavelength.
[d] CIE (x, y): Commission Internationale de l'Eclairage coordinates.
[e] FWHM: full width at half maximum.
[f] η_{ext}: external quantum efficiency; max: maximum.
[g] η_p: power efficiency; max: maximum.
[h] η_c: current efficiency; max: maximum.

of the former. At a current density of 100 mA cm^{-2}, they still retain promising performance: luminance (L)=2375 cd m^{-2}; external quantum efficiency (η_{ext})=2.4%; power efficiency (η_p)=1.0 lm W^{-1} and current efficiency (η_c)=2.4 cd A^{-1} for **BINAPC**, and luminance (L)=2835 cd m^{-2}, η_{ext}=2.3%; η_p=0.9 lm W^{-1} and η_c=2.8 cd A^{-1} for **BINAPN**. Use of the compounds as the host for phosphors should be also possible in view of the successful fabrication of OLEDs in this study.

3. Conclusions

In summary, we have developed two isomeric blue-emitting compounds consisting of arylamine and benzimidazole with a binaphthalene bridge. The new compounds exhibit bipolar transporting characteristics and can be used for efficient blue-emitting OLEDs. The use of highly twisted binaphthalene bridge results in partial disruption of π-conjugation. The difference in linking modes of the benzimidazole entity to the bridge, i.e., *C*-linkage (**BINAPC**) or *N*-linkage (**BINAPN**), leads to different photophysical and carrier-transport properties of the molecules. The *N*-linkage isomer has more balanced carrier mobilities.

4. Experimental section

4.1. General information

The ^{1}H NMR spectra were recorded on a Bruker AV III-400 MHz spectrometer, ^{13}C were recorded on a Bruker AV 500 MHz spectrometer and FAB-mass spectra were collected on a JMS-700 double focusing mass spectrometer (JEOL, Tokyo, Japan). Elemental analyses were performed on a Perkin–Elmer 2400 CHN analyzer. TGA and DSC were recorded on Perkin Elmer Pyris 1 TGA and DSC 7, respectively. Electronic absorption spectra were obtained on a Dynamica DB-20 UV–visible spectrometer. Emission spectra were recorded at room temperature by a Hitachi F-4500 FL spectrophotometer. Luminescence quantum yields (Φ_{PL}) were calculated relative to anthracene (Φ_{PL}=0.28 in ethanol).[27] Phosphorescence measurement was performed by Jobin Yvon FL3-21. Cyclic voltammetry experiments were performed with a CHI-621B electrochemical analyzer. All measurements were carried out at room temperature with a conventional three-electrode configuration consisting of a platinum working electrode, an auxiliary electrode, and a non-aqueous Ag/AgNO$_3$ reference electrode. The $E_{1/2}$ values were determined as 1/2(E^a+E^c), where E^a and E^c are the anodic and cathodic peak potentials, respectively. The solvent used was THF and the supporting electrolyte was 0.1 M tetrabutylammonium hexafluorophosphate. HOMOs were obtained from the measurement of ionization potential using low energy photoelectron spectrometer (RIKEN KEIKI AC II).

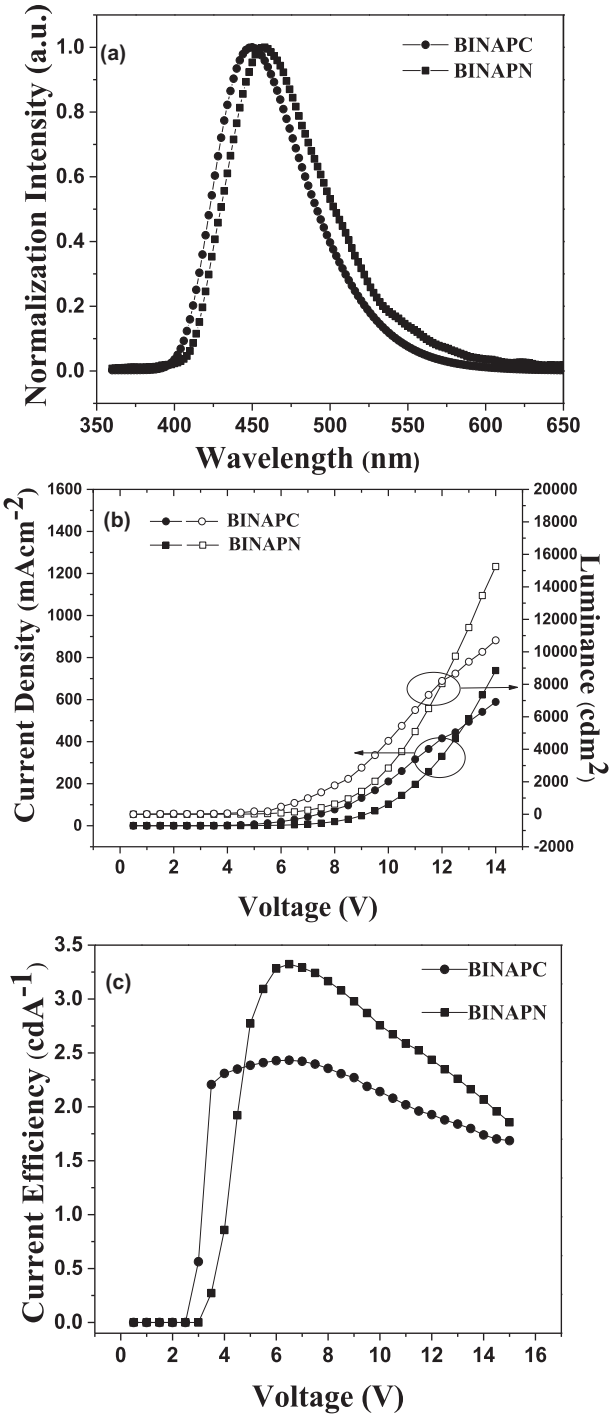

Fig. 5. EL performance of the device II for **BINAPC** and **BINAPN** (a) EL spectra. (b) Current density and luminance versus applied electric field c) Current efficiency versus voltage.

4.2. Material synthesis

Chemicals and solvents were reagent grades and purchased from Aldrich and Acros, respectively. Solvents were dried by standard procedures. All reactions and manipulations were carried out under N_2 with the use of standard inert atmosphere and Schlenk

techniques. All column chromatography was performed by using silica gel (230–400 mesh, Macherey–Nagel GmbH & Co.) as the stationary phase in a column, which is 25–35 cm in length and 2.5 cm in diameter. 2-(4-Bromophenyl)-1-phenyl-1*H*-benzo[*d*]imidazole (**1a**)[28] and 4′-bromo-*N*,*N*-diphenyl-[1,1′-binaphthalen]-4-amine[29] were synthesized according to literature methods. 1-(4-Bromophenyl)-2-phenyl-1*H*-benzo[*d*]imidazole (**1b**) was prepared as described in Scheme S1 (Supplementary data).

*4.2.1. 1-Phenyl-2-(4-(4,4,5,5-tetramethyl-1,3,2-dioxaborolan-2-yl) phenyl)-1H-benzo[d]imidazole (**2a**).* A mixture of **1a** (0.70 g, 2.0 mmol), bis(pinacolate)diborane (0.53 g, 2.1 mmol), l,l′-bis(diphenylphosphino) ferrocene]dichloropalladium (Pd(dppf)Cl_2) (0.060 g, 0.08 mmol), and anhydrous potassium acetate (0.393 g, 4.0 mmol) in 1,4-dioxane (20 mL) was heated at 80 °C under nitrogen for 12 h. After cooling to room temperature, the mixture was extracted with ethyl acetate (30 mL×3). The organic extracts were washed with water, brine, and then dried with anhydrous $MgSO_4$. After filtration, the filtrate was pumped dry in vacuo. The crude residue was subjected to column chromatography by eluting with hexanes/EA (8:1) as the eluent to give a white solid (yield: 81%). ^{1}H NMR (400 MHz, acetone-d_6): δ (ppm) 7.79 (d, *J*=7.6 Hz, 1H), 7.71 (d, *J*=7.6 Hz, 2H), 7.62–7.56 (m, 5H), 7.45 (d, *J*=7.6 Hz, 2H), 7.37–7.23 (m, 3H) and 1.34 (s, 12H); ^{13}C NMR (125 MHz, acetone-d_6): δ (ppm) 152.9, 144.3, 138.6, 138.2, 135.2, 134.0, 131.0, 129.7, 129.6, 128.6, 124.3, 123.7, 120.7, 111.4, 84.9, 25.3; Mass (FAB): *m*/*z*: 397.1 $[M+H]^+$.

*4.2.2. 2-Phenyl-1-(4-(4,4,5,5-tetramethyl-1,3,2-dioxaborolan-2-yl) phenyl)-1H-benzo[d]imidazole (**2b**).* Compound **2b** was synthesized by similar procedures as described for **2a**. The product was obtained as a white solid (yield: 43%). ^{1}H NMR (400 MHz, acetone-d_6): δ (ppm) 7.94 (d, *J*=6.4 Hz, 2H), 7.79 (d, *J*=7.6 Hz, 1H), 7.62–7.60 (m, 2H), 7.45 (d, *J*=8.0 Hz, 2H), 7.37–7.26 (m, 6H) and 1.34 (s, 12H); ^{13}C NMR (125 MHz, acetone-d_6): δ (ppm) 153.1, 144.3, 140.7, 138.3, 137.1, 131.4, 130.9, 130.4, 129.2, 128.6, 127.8, 124.2, 123.7, 120.6, 111.4, 85.09, 25.31; Mass (FAB): *m*/*z*: 397.2 $[M+H]^+$.

*4.2.3. N,N-Diphenyl-4′-(4-(1-phenyl-1H-benzo[d]imidazol-2-yl)phenyl)-[1,1′-binaphthalen]-4-amine (**BINAPC**).* 4′-Bromo-*N*,*N*-diphenyl-1,1′-binaphthyl-4-amine (1.0 g, 1.99 mmol), **2a** (0.79 g, 2.0 mmol), Pd(dppf)Cl_2 (82 mg, 0.1 mmol), and KF (0.35 g, 6.0 mmol) were dissolved in anhydrous DMF (20 mL) and the mixture was heated at 120 °C under nitrogen for 12 h. After cooling to room temperature, the mixture was extracted with ethyl acetate (30 mL×3). The organic extracts were washed with water, brine, and then dried with anhydrous $MgSO_4$. After filtration, the filtrate was pumped dry. The crude residue was subjected to column chromatography by using a mixture of hexanes/EA (8:1 to 6:1) as the eluent to give a yellow solid (yield: 68%). ^{1}H NMR (400 MHz, acetone-d_6): δ (ppm) 8.13 (d, *J*=8.0 Hz, 1H), 8.01 (d, *J*=8.0 Hz, 1H), 7.85–7.82 (m, 3H), 7.70–7.67 (m, 2H), 7.63–7.60 (m, 8H), 7.51 (d, *J*=7.6 Hz, 3H), 7.44–7.39 (m, 3H), 7.38–7.35 (m, 2H), 7.34–7.25 (m, 6H), 7.13 (d, *J*=8.4 Hz, 4H) and 7.02 (t, *J*=7.2 Hz, 2H); ^{13}C NMR (125 MHz, acetone-d_6): δ (ppm) 152.8, 149.7, 144.6, 144.5, 142.6, 140.3, 139.1, 138.8, 138.4, 137.8, 135.6, 134.2, 132.4, 132.3, 131.1, 130.9, 130.7, 130.4, 130.3, 129.8, 129.4, 128.8, 128.5, 127.9, 127.7, 127.5, 127.3, 127.1, 126.9, 125.5, 124.2, 123.7, 122.9, 120.7, 111.4; Mass (FAB): *m*/*z*: 689.2 $[M]^+$; Anal. Calcd for $C_{51}H_{35}N_3$; C, 88.79; H, 5.11; N, 6.09. Found: C, 88.70; H, 5.35; N, 6.30.

*4.2.4. N,N-Diphenyl-4′-(4-(2-phenyl-1H-benzo[d]imidazol-1-yl)phenyl)-[1,1′-binaphthalen]-4-amine (**BINAPN**).* **BINAPN** was synthesized by similar procedures as described for **BINAPC**. The product was obtained as a light green solid (yield: 43%). ^{1}H NMR (400 MHz, acetone-d_6): δ (ppm) 8.15 (d, *J*=8.4 Hz, 1H), 8.10 (d, *J*=8.4 Hz, 1H), 7.87–7.81 (m, 3H), 7.77–7.72 (m, 3H), 7.69–7.63 (m, 4H), 7.59–7.51 (m, 3H), 7.46–7.42 (m, 7H), 7.38–7.34 (m, 3H), 7.32–7.28 (m, 4H), 7.14 (d, *J*=8.0 Hz, 4H) and 7.03 (t, *J*=7.6 Hz, 2H); ^{13}C NMR (125 MHz, acetone-d_6): δ (ppm) 152.7, 149.7, 144.7, 144.5, 142.1, 140.0, 139.3, 138.6, 137.8, 137.6, 135.6, 134.3, 132.6, 132.3, 131.6, 130.5, 130.4, 130.3, 129.5, 129.3, 128.7, 128.6, 127.9, 127.8, 127.8, 127.5, 127.4, 127.4, 127.3, 126.9, 125.5, 124.3, 123.7, 123.0, 120.7, 111.5; Mass (FAB): *m*/*z*: 690.2 $[M+H]^+$; Anal. Calcd for $C_{51}H_{35}N_3$: C, 88.79; H, 5.11; N, 6.09. Found: C, 88.74; H, 5.31; N, 6.05.

4.3. Light-emitting devices fabrication

Pre-patterned ITO substrates were cleaned by standard procedure before use. Single-layered EL devices were prepared by vacuum deposition of 80 nm of **BINAPC** or **BINAPN** as emitting layer. Three-layered EL devices were fabricated by vacuum deposition of 30 nm of NPB, followed by 20 nm of **BINAPC** (or **BINAPN**) and 30 nm of TPBI as hole-transporting, light-emitting and electron-transporting layers, respectively. LiF (1 nm thick) was then deposited as the buffer layer. Aluminum was finally deposited as the cathode (100 nm). Electroluminescence (EL) spectra were recorded on a Hitachi fluorescence spectrophotometer F-4500. *I*–*V* curves were measured by using photodiode detector (GW INSTEK, GPC-3030DQ) under ambient environment.

4.4. Time-of-flight (TOF) mobility measurements

The mobilities of compounds were characterized by the transient photocurrent technique, i.e., the time-of-flight (TOF) technique.[30] The TOF measurement were performed using the sample structure of: glass/Ag (30 nm)/**BINAPC** or **BINAPN** (1–2 μm)/Al (150 nm) with an active area of 2×2 mm^2 as described in a previous report. The organic layer was deposited by vacuum deposition. In the TOF measurement, a frequency-tripled Nd:YAG laser (355 nm) with ~10 ns pulse duration was used for pulsed illumination through the semi-transparent Ag. Under an applied DC bias, the transient photocurrent as a function of time was recorded with a digital storage oscilloscope. The TOF measurements were typically performed in a 10^{-5} Torr vacuum chamber. Depending on the polarity of the applied bias *V*, selected photogenerated carriers (holes or electrons) are swept across the sample thickness *D* with a transit time t_T, the applied electric field *E* is then *V*/*D*, and the carrier mobility is given by$=D/(t_T \cdot E)=D^2/(V \cdot t_T)$.

4.5. Quantum chemistry computation

The geometries and electronic structures of **BINAPC** and **BINAPN** were calculated using density functional theory (DFT). All structures in their ground-state were optimized at B3LYP/6-311G** level of theory. The results are with a positive definite Hessian. The singlet excited state and HOMO/LUMO energies were optimized using ωPBE with 6-311G* basis set to analyze the effect of the linking topologies in electronic properties. The lowest singlet excitation (S_1) of the compounds was calculated using time-dependent density functional theory (TDDFT) at ωPBE/6-311G* level.

Acknowledgements

We would like to thank you to Dr. Zhi-Qiang Wesley You and Dr. Hsien-Hsin Chou for providing the quantum calculation data and discussion.

Supplementary data

Supplementary data related to this article can be found at http://dx.doi.org/10.1016/j.tet.2014.03.017.

References and notes

1. (a) Holder, E.; Langeveld, B. M. W.; Schubert, U. *Adv. Mater.* **2005**, *17*, 1109–1211; (b) Kim, S.; Kwon, H. J.; Lee, S.; Shim, H.; Chun, Y.; Choi, W.; Kwack, J.; Han, D.; Song, M.; Kim, S.; Mohammadi, S.; Kee, I.; Lee, S. Y. *Adv. Mater.* **2011**, *23*, 3511–3516.
2. Li, R. Z.; Meng, H. *Organic Light-Emitting Materials and Devices*; Taylor & Francis, 2010, Vol. 1, pp 1–639.
3. Sasabe, H.; Kido, J. *Chem. Mater.* **2011**, *23*, 621–630.
4. Shirota, Y. *J. Mater. Chem.* **2005**, *15*, 75–93.
5. Shirato, Y. In *Organic Light Emitting Devices: Synthesis, Properties and Applications*; Mullen, K., Scherf, U., Eds.; Wiley-VCH: 2006; Vol. 1, pp 245–261.
6. Gong, L. Z.; Hu, Q. S.; Pu, L. *J. Org. Chem.* **2001**, *66*, 2358–2367.
7. Pu, L. *Chem. Rev.* **1998**, *98*, 2405–2494.
8. Van Elshocht, S.; Verbiest, T.; Kauranen, M.; Liang, M.; Hua, C.; Musick, K. Y.; Lin, P.; Persoons, A. *Chem. Phys. Lett.* **1999**, *309*, 315–320.
9. (a) Wei, B.; Liu, J. Z.; Zhang, Y.; Zhang, J. H.; Peng, H. N.; Fan, H. L.; He, Y. B.; Gao, X. C. *Adv. Funct. Mater.* **2010**, *20*, 2448–2458; (b) Zhou, Y.; He, Q. G.; Yang, Y.; Zhong, H. Z.; He, C.; Sang, G. Y.; Liu, W.; Yang, C. H.; Bai, F. L.; Li, Y. F. *Adv. Funct. Mater.* **2008**, *18*, 3299–3306; (c) Zheng, L. X.; Urian, R. C.; Liu, Y. Q.; Jen, A. K. Y.; Pu, L. *Chem. Mater.* **2000**, *12*, 13–15.
10. Ostrowski, J. C.; Hudack, R. A.; Robinson, M. R.; Wang, S. J.; Bazan, G. C. *Chem.—Eur. J.* **2001**, *7*, 4500–4511.
11. (a) Chen, C. H.; Huang, W. S.; Lai, M. Y.; Tsao, W. C.; Lin, J. T.; Wu, Y. H.; Ke, T. H.; Chen, L. Y.; Wu, C. C. *Adv. Funct. Mater.* **2009**, *19*, 2661–2670; (b) Hung, W. Y.; Chi, L. C.; Chen, W. J.; Mondal, E.; Chou, S. H.; Wong, K. T.; Chi, Y. *J. Mater. Chem.* **2011**, *21*, 19249–19256.
12. Duan, L. A.; Qiao, J. A.; Sun, Y. D.; Qiu, Y. *Adv. Mater.* **2011**, *23*, 1137–1144.
13. Chaskar, A.; Chen, H. F.; Wong, K. T. *Adv. Mater.* **2011**, *23*, 3876–3895.
14. Huang, J.; Su, J. H.; Li, X.; Lam, M. K.; Fung, K. M.; Fan, H. H.; Cheah, K. W.; Chen, C. H.; Tian, H. *J. Mater. Chem.* **2011**, *21*, 2957–2964.
15. (a) Zhao, Z.; Zhang, F. J.; Zhang, X.; Yang, X. D.; Li, H. X.; Gao, X. K.; Di, C. A.; Zhu, D. B. *Macromolecules* **2013**, *46*, 7705–7714; (b) Zhao, Z.; Wang, Z. L.; Hu, Y. B.; Yang, X. D.; Li, H. X.; Gao, X. K.; Zhu, D. B. *J. Org. Chem.* **2013**, *78*, 12214–12219.
16. (a) Chen, Y. M.; Hung, W. Y.; You, H. W.; Chaskar, A.; Ting, H. C.; Chen, H. F.; Wong, K. T.; Liu, Y. H. *J. Mater. Chem.* **2011**, *21*, 14971–14978; (b) Chou, S. H.; Hung, W. Y.; Chen, C. M.; Liu, Q. Y.; Liu, Y. H.; Wong, K. T. *RSC Adv.* **2013**, *3*, 13891–13900; (c) Varathan, E.; Vijay, D.; Kumar, P. S. V.; Subramanian, V. *J. Mater. Chem. C* **2013**, *1*, 4261–4274.
17. Jo, W. J.; Kim, K. H.; No, H. C.; Shin, D. Y.; Oh, S. J.; Son, J. H.; Kim, Y. H.; Cho, Y. K.; Zhao, Q. H.; Lee, K. H.; Oh, H. Y.; Kwon, S. K. *Synth. Met.* **2009**, *159*, 1359–1364.
18. Ge, Z. Y.; Hayakawa, T.; Ando, S.; Ueda, M.; Akiike, T.; Miyamoto, H.; Kajita, T.; Kakimoto, M. A. *Adv. Funct. Mater.* **2008**, *18*, 584–590.
19. Gong, S. L.; Chen, Y. H.; Yang, C. L.; Zhong, C.; Qin, J. G.; Ma, D. G. *Adv. Mater.* **2010**, *22*, 5370–5373.
20. Chien, Y. Y.; Wong, K. T.; Chou, P. T.; Cheng, Y. M. *Chem. Commun.* **2002**, 2874–2875.
21. Lakowicz, J. R. *Principles of Fluorescence Spectroscopy*, 3rd ed.; Spinger, 2006; pp 1–351.
22. Lai, M. Y.; Chen, C. H.; Huang, W. S.; Lin, J. T.; Ke, T. H.; Chen, L. Y.; Tsai, M. H.; Wu, C. C. *Angew. Chem., Int. Ed.* **2008**, *47*, 581–585.
23. (a) Bassler, H. *Int. J. Mod. Phys. B* **1994**, *8*, 847–854; (b) Arkhipov, V. I.; Bassler, H.; Rudenko, A. I. *Philos. Mag. B* **1992**, *65*, 615–619; (c) Gill, W. D. *J. Appl. Phys.* **1972**, *43*, 5033–5040.
24. Lin, L. B.; Young, R. H.; Mason, M. G.; Jenekhe, S. A.; Borsenberger, P. M. *Appl. Phys. Lett.* **1998**, *72*, 864–866.
25. Li, Y. Q.; Fung, M. K.; Xie, Z. Y.; Lee, S. T.; Hung, L. S.; Shi, J. M. *Adv. Mater.* **2002**, *14*, 1317–1321.
26. (a) Shirota, Y. *J. Mater. Chem.* **2000**, *10*, 1–25; (b) Kulkarni, A. P.; Tonzola, C. J.; Babel, A.; Jenekhe, S. A. *Chem. Mater.* **2004**, *16*, 4556–4573; (c) Shirota, Y.; Kageyama, H. *Chem. Rev.* **2007**, *107*, 953–1010; (d) Hertel, D.; Bassler, H. *ChemPhysChem* **2008**, *9*, 666–688.
27. Brouwer, A. M. *Pure Appl. Chem.* **2011**, *83*, 2213–2228.
28. Huang, W. S.; Lin, J. T.; Lin, H. C. *Org. Electron.* **2008**, *9*, 557–568.
29. Chen, Y. C.; Chen, Y. H.; Chou, H. H.; Chaurasia, S.; Wen, Y. S.; Lin, J. T.; Yao, C. F. *Chem.—Asian J.* **2012**, *7*, 1074–1084.
30. (a) Wu, C. C.; Liu, T. L.; Hung, W. Y.; Lin, Y. T.; Wong, K. T.; Chen, R. T.; Chen, Y. M.; Chien, Y. Y. *J. Am. Chem. Soc.* **2003**, *125*, 3710–3711; (b) Chen, L. Y.; Hung, W. Y.; Lin, Y. T.; Wu, C. C.; Chao, T. C.; Hung, T. H.; Wong, K. T. *Appl. Phys. Lett.* **2005**, *87*, 112103–112103-3; (c) Wu, C. C.; Hung, W. Y.; Liu, T. L.; Zhang, L. Z.; Luh, T. Y. *J. Appl. Phys.* **2003**, *93*, 5465–5471; (d) Borsenberger, M. P.; Weiss, S. D.; *Organic Photoreceptors for Imaging Systems*, 1st ed.; CRC, 1998, Vol. 1, pp 1–407.